Numerical Verification of Stainless Steel Overall Buckling Curves

Petr Hradil, Asko Talja

VTT, Technical Research Centre of Finland, P.O. Box 1000, FI-02044 VTT, Finland

Abstract

The introduction of new material grades or fabrication methods in engineering structures always raises concerns about the validity of current design rules, especially those based on earlier material or member testing. One of the fundamental structural checks is the overall stability of beams and columns. In this paper, a series of virtual buckling tests is calculated and compared to the Eurocode buckling curves. The main focus is on the applicability of ferritic steels that generally have different stress-strain behaviour than austenitic or duplex grades.

Keywords

Stainless steel, buckling, finite element method, stress-strain relation, regression

Highlights

Over 1,500 numerical calculations of models with shell elements, residual stress and nonlinear materials were carried out. ·Software for virtual testing in Abaqus was developed and used for this study. ·The recorded ultimate loads were recalculated to non-dimensional reduction factors. ·The results were compared to the standard Eurocode 3 buckling curves.

1 Introduction

Ferritic stainless steels are very competitive materials for load-bearing building structures, but they do not have such a long tradition as austenitic grades and a relatively low amount of experimental results from members is available to support design rules for such materials. The geometrically and materially nonlinear analysis on imperfect finite element models (GMNIA) has a great potential to simulate real experiments and, for instance, to computationally predict the buckling curve of a certain material and cross-section including the effects of fabrication such as enhanced strength and residual stress. The parametrical study was carried out to obtain parameters for overall buckling reduction calculation and was compared to the experimental tests [1-9] and Eurocode 3 buckling curves. Based on the review of available data [10], a preliminary numerical study [11,12] and experiments [6], several important parameters were recognised that have to be taken into account in this study.

(a) Buckling modes

The study covers flexural buckling (FB) to the major and minor axes, torsional-flexural buckling (TFB) and lateral-torsional buckling of beams (LTB). These modes are also recognised in Eurocode 3, where the reduction factors are given separately for compressed columns and members subjected to bending.

(b) Cross-sectional shapes and fabrication methods

Cold-formed open sections, hollow sections and welded open sections are the basic categories in Eurocode 3, Part 1-4. We selected cold-rolled (by circle-to-rectangle forming) hollow sections, press-braked open sections and welded I-sections in the present study because more detailed knowledge of the fabrication method was needed for accurate buckling strength prediction.

(c) Material nonlinearity

The value of the Ramberg-Osgood coefficient n is generally higher in ferritic steels (black markers in Figure 1) but it can decrease during fabrication. It should be noted that a higher nonlinear factor usually leads to a higher buckling strength [11-13].

(d) Strain hardening rate

The stress-strain relation beyond the yield point can be represented as the ratio of the ultimate stress σ_u or 1% proof stress $\sigma_{1.0}$ and 0.2% proof stress $\sigma_{0.2}$. This parameter does not significantly affect the buckling strength, but the lower hardening rate also means lower strength enhancement in corners, which can lead to differences in the average member strength. We extrapolated the collected experimental stress-strain curves to 40% strain and used the corresponding stress σ_{40} in Figure 1 instead of the real measured ultimate stress because the value of ultimate strain ε_u in the numerical models is always 40%. The lower limit of f_u/f_y ratio of stainless steels in Eurocode 3 is 1.1.

(e) Design yield strength

The particular value of yield strength used in the member design does not significantly affect the buckling reduction factors, but it is essential to know to which of the following strengths it corresponds. Cold-formed profiles from sheets

with virgin material strength $\sigma_{0.2,v}$ may have higher values of yield point in the flat parts $\sigma_{0.2,f}$ and corners $\sigma_{0.2,c}$ due to the fabrication. Therefore, the average yield strength $f_{y,a}$ can differ from the basic one $f_{y,b}$ and would require a new set of buckling curves.

2 Materials and Cross-sections

The effect of material nonlinearity and work-hardening from the fabrication is described by two important material parameters: the nonlinear factor n and the ratio of ultimate and yield strength $f_u/f_y = \sigma_u/\sigma_{0.2}$.We used four groups of materials with different nonlinear factor n (groups A, B, C and D) varying from 5 to 40 and four levels of material hardening (groups 1, 1*, 2 and 2*) from 1.1 to 1.8. Their properties correspond to the basic materials in press-braked and welded sections and to the flat part materials in case of cold-rolled hollow sections. The initial modulus of elasticity E_0 was always 200 GPa and the basic (flat parts) yield strength $\sigma_{0.2}$ was selected as low as 250 MPa to produce conservative results. Stress-strain relationships are based on Mirambell and Real's two stage model [14], where the ultimate strain ε_u and the second nonlinear parameter m are 0.4 and 3 respectively in all cases. The 1.0% proof stress $\sigma_{1.0}$, the ultimate strength σ_u and the nonlinear parameter n are presented in Table 1.

Table 1 Variable material properties

Material	$\sigma_{1.0}$ (MPa)	σ_u (MPa)	n	Material	$\sigma_{1.0}$ (MPa)	σ_u (MPa)	n
A1	256.25	275	5	A2	275	350	5
B1	256.25	275	10	B2	275	350	10
C1	256.25	275	20	C2	275	350	20
D1	256.25	275	40	D2	275	350	40
A1*	262.5	300	5	A2*	300	450	5
B1*	262.5	300	10	B2*	300	450	10
C1*	262.5	300	20	C2*	300	450	20
D1*	262.5	300	40	D2*	300	450	40

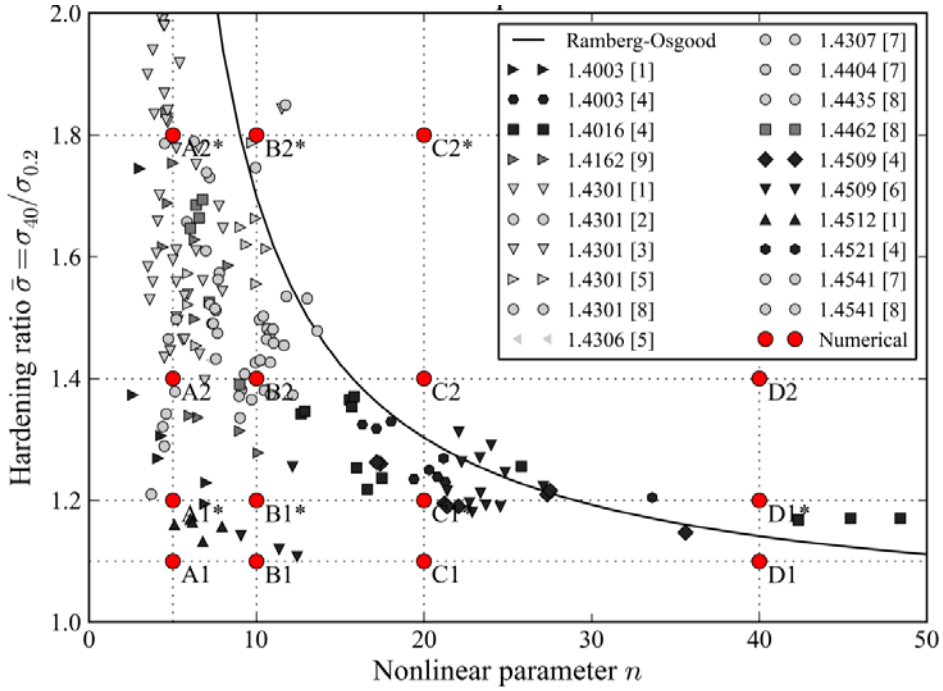

Figure 1 Nonlinear factor and hardening ratio in collected material tests (black markers represent ferritic grades, light grey markers austenitic materials and dark grey markers indicate duplex steels)

The study focuses on welded sections (I and H profiles), press-braked open sections (C-sections) and cold-rolled hollow sections (SHS and RHS). One cross-section was selected from each group with high A/W ratio to provide conservative results (see Figure 2 and Table 2). This ratio was always higher than in experiments reported in the commentary to the Design Manual for Structural Stainless Steel [15] and represented the higher boundary in the collected database of typical cross-sectional shapes. Sectional properties of welded I-sections were compared to the parameters of typical hot-rolled steel profiles (IPE and HE) and cold-formed cross-section geometrical properties are based on more than 800 cross-sectional shapes from EN 1019-2, SCI report [16] and Stalatube Oy data sheets [17]. Table 2 also shows additional important cross-sectional parameters such as the internal corner radius and thickness ratio r_i/t and the share of a cross-sectional area with enhanced material properties A_{enh}.

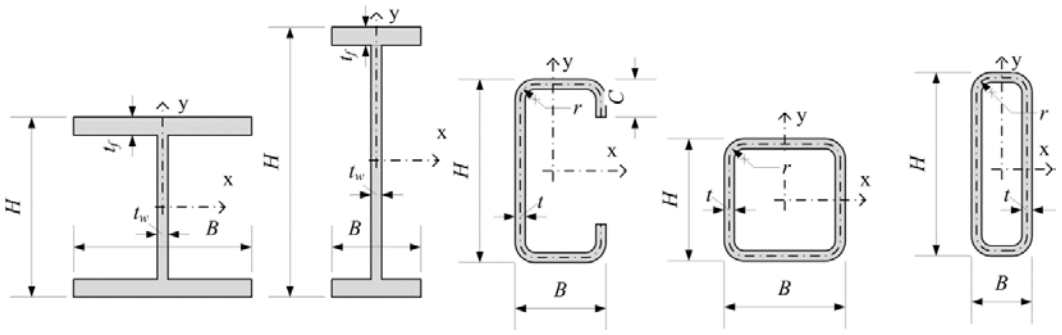

Figure 2 Cross-section types used in the study

Table 2 Cross-sectional parameters

Section	H (mm)	B (mm)	C (mm)	t_w (mm)	t_f (mm)	$A/W_{el,x}$ (cm^{-1})	$A/W_{el,y}$ (cm^{-1})	r_i/t	A_{enh}/A
I 150x50	150	50	-	5	10	0.21	1.97	-	-
H 100x100	100	100	-	5	10	0.28	0.72	-	-
C 72x36x4	72	36	15	4		0.47	1.30	1.0	24%
RHS 72x24x4	72	24	-	4		0.60	1.30	1.0	52%
SHS 48x4	48	48	-	4		0.69	0.69	1.0	62%

3 Finite element models

The numerical models were created and evaluated using the Abauqs plugin developed to simulate virtual testing of cold-formed steel members [18]. The functionality of the plugin was extended by script that automatically executed batches of pre-defined models with variable member lengths, evaluated results and plotted buckling curves.

3.1 Enhanced material strength

The enhanced yield strength of press-braked open section C 72x36x4 was applied in the corners according to Cruise and Gardner's model [19] in Eq. (1).

$$\sigma_{0.2,c} = \frac{1.673\,\sigma_{0.2}}{(r_i/t)^{0.126}} \quad (1)$$

The average yield strength $f_{y,a}$ is therefore 294 MPa in the selected section where r_i/t = 1.0 and A_{enh}/A = 24%.

Cold-rolled hollow sections RHS 72x24x4 and SHS 48x4 have a larger area affected by the fabrication, which extends $2t$ from the corners to the flat parts. The current predictive models for the enhanced strength in corners $\sigma_{0.2,c}$ and flat faces $\sigma_{0.2,f}$ of hollow sections are based on the knowledge of virgin material yield strength $\sigma_{0.2,v}$. Moreover, the model proposed by Cruise and Gardner [19] for hollow sections is limited to either low A/W or high f_u/f_y ratios, which was not acceptable in our study. Therefore we used Rossi's prediction [20] in Eq. (2) with the virgin material yield strength varying from 175 to 235 MPa that produced a flat part strength of exactly 250 MPa and a yield strength in the corners between 290 and 585 MPa. The calculation of parameters C_1, C_2 and α is described in [20].

$$\sigma_{0.2,c} = \sigma_{0.2,v} + \frac{\sigma_{u,v}}{C_1\left(\frac{r_i}{t/2}\right) + C_2\left(\frac{r_i}{t/2}\right)^{\alpha}} \text{ and } \sigma_{0.2,f} = \sigma_{0.2,v} + \frac{\sigma_{u,v}}{C_1\left[\frac{(b+d)/\pi}{t/2}\right] + C_2\left[\frac{(b+d)/\pi}{t/2}\right]^{\alpha}} \quad (2)$$

3.2 Residual stresses

Membrane stresses from welding were considered in the I and H sections. The model for carbon steels from the Swedish standard BSK 99 that was proposed by Gardner and Cruise [21] for ferritic fabricated sections was used, where the compressive stress σ_c is calculated to maintain the equilibrium (Eq. (3)). The compressive stress was therefore 92.5 and 72.6 MPa in I and H sections respectively.

$$\sigma_c = \frac{2.25(t_f + t_w)}{B + 0.5H - 2.25(t_f + t_w)}\sigma_{0.2} \quad (3)$$

Bending residual stresses of 36% of basic yield strength $f_{y,b}$ were inserted in corner areas and 15% of $f_{y,b}$ in flats according to Gardner and Cruise [21] in press-braked open sections. In the case of hollow sections, the highest level of

bending residual stresses in corners and flat parts was 37% and 63% respectively. Membrane stresses were neglected in both types of cold-formed sections according to [21].

3.3 Initial imperfections

All finite element models were perturbed prior to the arc-length nonlinear calculation. The initial imperfections were distributed according to the first overall buckling shape with positive critical load produced by the linear eigenvalue analysis (LEA). The search for such shape can be unsuccessful due to very low member slenderness; therefore we used constrained models according to the study by Zhang and Tong [22], which also provided results for members where local or distortional buckling dominated.

The fabrication tolerance $L/750$ was used as the imperfection amplitude in the preliminary study [11]. Since residual stresses are included in FE models this time, lower amplitude was needed that represents only the pure geometrical imperfections. We selected $L/1500$, which is widely used in similar studies [23,24].

4 Methods

Numerical models of full-section tension tests with enhanced material properties and residual stresses were calculated before the buckling curves were evaluated, in order to verify the predicted average yield strength $f_{y,a}$ and reduced nonlinear factor n. Changes in material nonlinearity due to cold-forming would affect the estimated impact of the original n factor on the buckling curve. In compression or bending tests simulations, ten points of each buckling curve were calculated with the nondimensional slenderness λ ranging from 0.18 to 4.0. The nonlinear regression analysis provided parameters α and λ_0 for the Ayrton-Perry curve [25] fitted to the calculated points (see Figure 3).

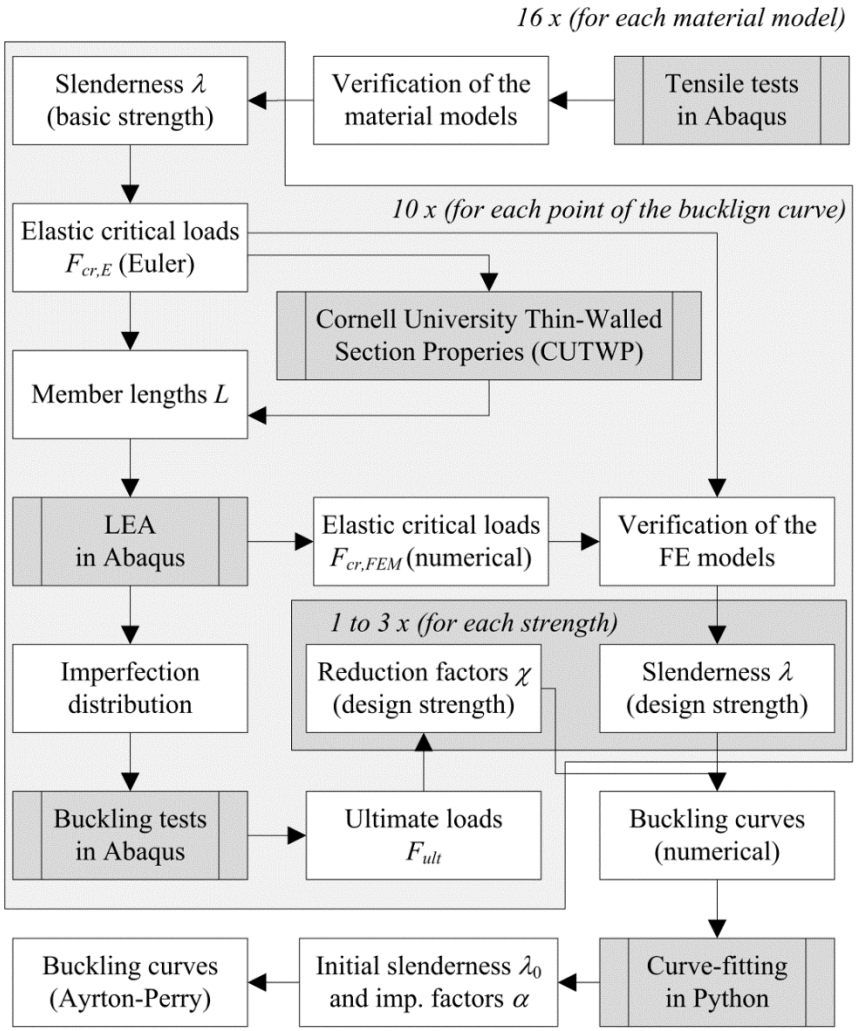

Figure 3 Numerical verification of Eurocode buckling curves

(a) Tensile tests

One metre long members with no initial geometrical imperfections were loaded in tension and the load-displacement relation was recorded. The stress-strain curve obtained from the numerical results was compared to the original constitutive model. The least square optimisation tool described in Appendix E of VTT's report [6] generated the real

yield strength and nonlinear parameter *n* of the whole cross-section. The calculated strength was then compared to that predicted by Rossi's model [20].

(b) Nondimensional slenderness $\lambda_{f(b)}$

Ten values of nondimensional slenderness were selected from 0.18 to 4.00 in the sequence $\lambda_{f(b)} = \sqrt{2}^{N}$ for *N* from -5 to 4. They are assumed to be valid in combination with the basic (or flat parts) strength 250 MPa.

(c) Elastic critical loads $F_{cr,E}$ ($M_{cr,E}$)

The theory of elastic buckling was used to predict the value of the critical load for compressed members and members subjected to bending according to Eq. (4) where *A* and *W* were the cross-sectional area and section modulus respectively.

$$F_{cr,E} = \frac{f_{y,f(b)} A}{\lambda_{f(b)}^2} \text{ and } M_{cr,E} = \frac{f_{y,f(b)} W}{\lambda_{f(b)}^2} \quad (4)$$

(d) Member lengths *L*

The length of the member was calculated directly in simple flexural buckling cases (Eq. (5)) or with CUTWP software [26] in more complex torsional buckling cases using the iterative approach.

$$L = \lambda_{f(b)} \cdot \pi i \sqrt{E / f_{y,f(b)}} = \pi \sqrt{EI / F_{cr,E}} \quad (5)$$

(e) Elastic critical loads $F_{cr,FEM}$ ($M_{cr,FEM}$)

The critical load from the linear eigenvalue analysis (LEA) of the model with non-uniform distribution of material properties and residual stresses does not necessarily have to be the same as the predicted one. Both results were compared, and when their difference was higher than 5%, the basic nondimensional slenderness was corrected using Eq. (6).

(f) Nondimensional slenderness λ_v, $\lambda_{f(b)}$ and λ_a

Each type of yield strength other than the basic one (virgin or average) which can be used in design would require different buckling curves to be plotted. Therefore the values of nondimensional slenderness were corrected accordingly using Eq. (6) where f_y stands for the virgin material strength $f_{y,v}$, basic (flat parts) strength $f_{y,f(b)}$ or the average strength $f_{y,a}$.

$$\lambda = \sqrt{f_y A / F_{cr,FEM}} \text{ and } \lambda = \sqrt{f_y W / M_{cr,FEM}} \quad (6)$$

(g) Imperfection distribution

The shapes of initial imperfections were extracted from the results of LEA analysis and amplified to match selected amplitude *L*/1500 in the node with the highest displacement.

(h) Ultimate loads F_{ult} (M_{ult})

The peak loads in arc-length Riks analysis [27] were recorded for each evaluated case. This is the common approach in geometrically and materially nonlinear analysis of imperfect models (GMNIA).

(i) Nondimensional reduction factors χ

The value of the reduction factor has to correspond to the yield strength that is used in the design or higher to provide safe results. Therefore it was possible to create three sets of reduction factor-to-slenderness plots for $f_{y,a}$ (average strength), $f_{y,f}$ (flat faces) and virgin material strength $f_{y,v}$ of cold-rolled hollow sections according to Eq. (7). Press-braked open sections yielded two sets of buckling curves with the average and basic strength $f_{y,b,}$ and only one basic strength was needed for the welded open sections.

$$\chi = F_{ult} / f_y A \text{ and } \chi = M_{ult} / f_y W \quad (7)$$

(j) Buckling curves

Nondimensional reduction factors were plotted against nondimensional slenderness and formed the approximation of 208 buckling curves (48 for welded open sections, 64 for press-braked open sections and 96 for cold-rolled hollow sections). The same least square optimisation method as described in the tensile tests was applied to the calculated sets of nondimensional parameters. Finally, the values of the buckling curve parameters were selected to match the current Eurocode buckling curves, where the initial slenderness is either 0.2 or 0.4, and the imperfection factor is 0.21, 0.34, 0.49 or 0.76.

5 Results and Discussion

5.1 Tensile tests

The nonlinearity of axially-loaded member load-displacement relation increases during cold forming; therefore we expected a lower nonlinear factor for the whole cross-section than in the original material. This effect can be verified by a simple tensile test of the whole cross-section. Using the finite element method, we were able to estimate how much the nonlinearity was affected by enhanced material properties and how big the effect of residual stress was. Table 3 shows curve-fitted results of an average material yield strength $\sigma_{0.2,TT}$ and nonlinear factor n_{TT} from full-section tensile tests with and without residual stresses.

Table 3 Curve-fitted parameters of stress-strain curves from the full-section tests

Cross-section	Material		with residual stress		without residual stress	
		n	$\sigma_{0.2,TT}$ (MPa)	n_{TT}	$\sigma_{0.2,TT}$ (MPa)	n_{TT}
C 72x34x4	A2	5	294.3	4.63	294.9	4.72
	B2	10	296.3	8.04	296.7	8.58
	C2	20	297.3	12.73	297.6	15.03
SHS 48x4	A2	5	275.4	4.96	276.4	4.94
	B2	10	275.5	7.49	276.5	9.63
	C2	20	275.7	12.02	276.3	17.89
RHS 72x24x4	A2	5	272.5	4.99	273.0	4.95
	B2	10	271.7	7.59	272.7	9.60
	C2	20	271.8	12.14	272.4	17.99

As can be seen in Table 3, differences between nonlinear factors decreased partly because of residual stress and partly due to the non-uniform material distribution. Smaller effect of n factor than in the preliminary study [11,12], where the fabrication was not considered, is then expected especially in hollow sections.

5.2 Buckling tests

Calculated lengths of columns and beams are presented in Table 4. These members were loaded with concentric axial force or end-moments according to their expected failure mode. Pinned-pinned supports and concentric axial loading were applied in the flexural buckling study. The single-symmetric members were forced to fail in torsional-flexural buckling, fixing both ends in minor axis bending, torsion and warping. In the case of lateral-torsional buckling, members were simply supported and loaded with end-moments. Both ends were additionally restrained against torsion and warping. Table 5 shows the ultimate loads of GMNIA calculations.

Table 4 Lengths of tested members in mm

$\lambda_{f(b)}$	H 100x100	I 150x50		C 72x34x4		SHS 48x4	RHS 72x24x4
	FB maj.	FB min.	LTB	FB min.	TFB	FB maj.	FB min.
0.18	663	174	301	196	282	292	151
0.25	938	247	430	278	401	413	213
0.35	1327	349	618	393	576	584	302
0.50	1876	493	904	555	838	826	427
0.71	2653	697	1365	785	1251	1168	603
1.00	3752	986	2183	1111	1923	1652	853
1.40	5307	1395	3802	1570	2981	2336	1207
2.00	7505	1973	7170	2221	4477	3304	1706
2.80	10613	2790	14066	3141	6536	4672	2413
4.00	15010	3945	28000	4442	9390	6607	3413

Table 5 Minimum ultimate loads in kN in compression and kNm in bending tests

$\lambda_{f(b)}$	H 100x100	I 150x50		C 72x34x4		SHS 48x4	RHS 72x24x4
	FB maj.	FB min.	LTB	FB min.	TFB	FB maj.	FB min.
0.18	599.7	422.4	23.54	166.6	172.9	175.6	175.1
0.25	593.4	411.8	23.01	162.5	170.7	163.0	163.8
0.35	574.8	390.6	22.12	155.3	165.8	154.1	152.1
0.50	522.2	344.1	20.25	142.8	154.6	141.4	142.1
0.71	428.6	269.2	16.74	120.7	130.9	119.8	124.1
1.00	300.9	184.9	12.39	89.9	96.4	87.9	91.1
1.40	189.8	114.4	8.00	57.6	59.5	52.4	54.9
2.00	109.7	65.9	4.41	32.5	32.4	28.5	28.8
2.80	59.3	35.9	2.27	17.0	16.7	14.5	14.4
4.00	30.9	19.0	n/a	8.7	8.5	5.4	5.5

5.3 Reduction factors

Nondimensional reduction factors were calculated for all materials and all types of yield strength. Here, we present the most important results with the basic or flat part strengths that are currently used in the Eurocode 3, Part 1-4. Figures 4 to 10 show the calculated numerical results for all materials and basic or flat part strength. The effect of using virgin material strength of cold-rolled hollow sections or using average strength of press-braked and cold-rolled sections is briefly described in this chapter. Presented curves are overlapping in some cases due to very small differences between reduction factors of welded and press-braked sections with materials with the same f_u/f_y ratio. Numerical results are compared to the Eurocode 3 buckling curves for stainless steels (EN 1993-1-4) and carbon steels (EN 1993-1-1 and EN 1993-1-3) according to Table 6.

Table 6 Imperfection factors α and initial slenderness λ_0 of Eurocode 3 buckling curves

	H 100x100	I 150x50		C 72x34x4		SHS 48x4	RHS 72x24x4
	FB maj.	FB min.	LTB	FB min.	TFB	FB maj.	FB min.
EN 1993-1-4: Supplementary rules for stainless steels							
α	0.49	0.76	0.76	0.49	0.34	0.49	0.49
λ_0	0.2	0.2	0.4	0.4	0.2	0.4	0.4
EN 1993-1-1: General rules and rules for buildings							
EN 1993-1-3: Supplementary rules for cold formed members and sheeting							
α	0.34	0.49	0.76	0.34	0.34	0.49	0.49
λ_0	0.2	0.2	0.2	0.2	0.2	0.2	0.2

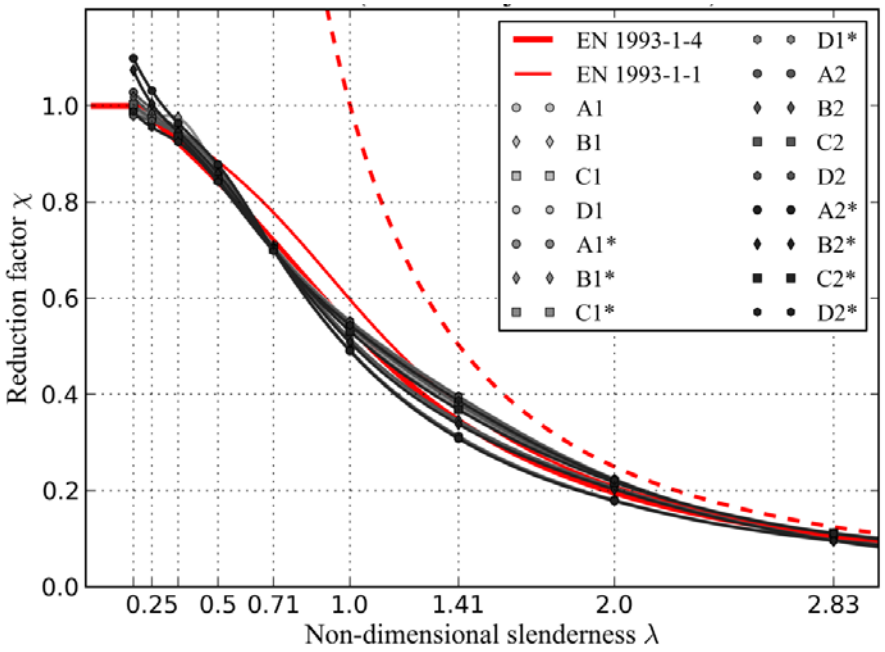

Figure 4 H 100x100 flexural buckling - major axis

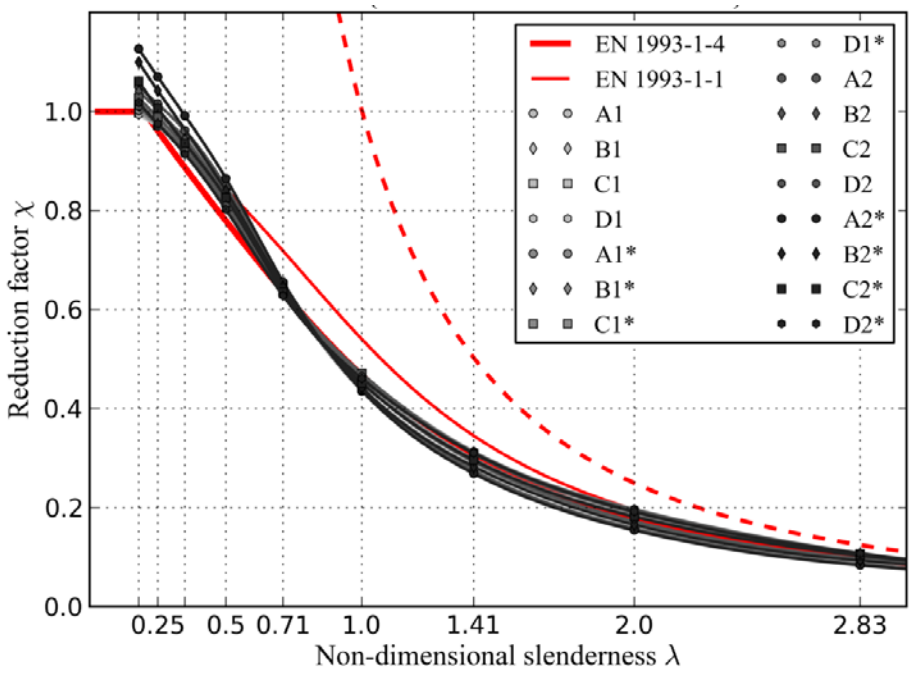

Figure 5 I 150x50 flexural buckling - minor axis

Calculated reduction factors of welded open sections indicate that the flexural buckling to the major or minor axis (Figures 4 and 5) corresponds to the EN 1993-1-4 buckling curves. Higher *n* values may yield in a slight improvement in buckling resistance for higher slenderness levels than 0.71.

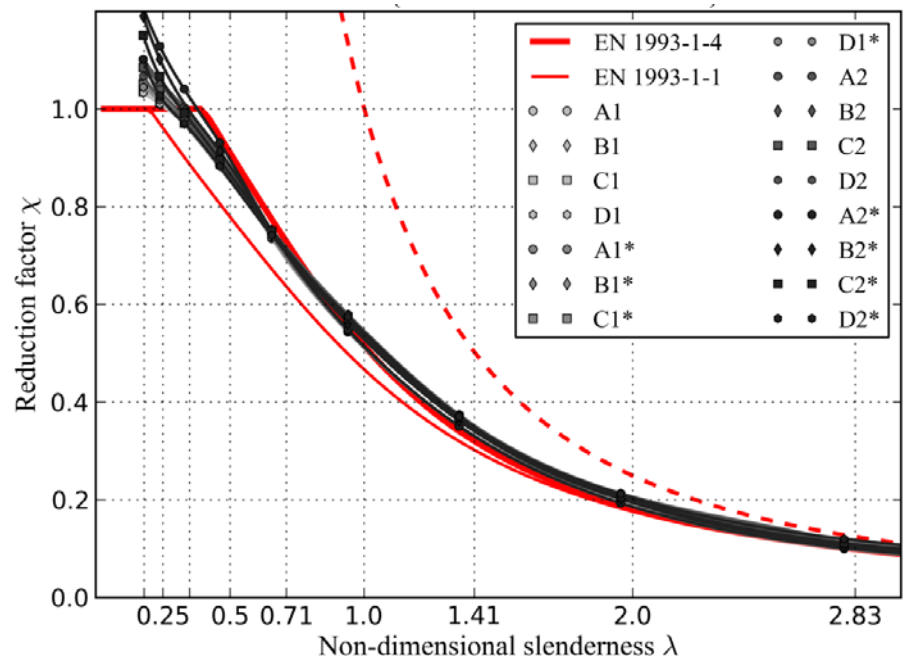

Figure 6 I 150x50 lateral-torsional buckling

Lateral-torsional buckling tests resulted in good correlation to the EN 1993-1-4 when the plastic section modulus was used, and therefore are conservative in elastic design.

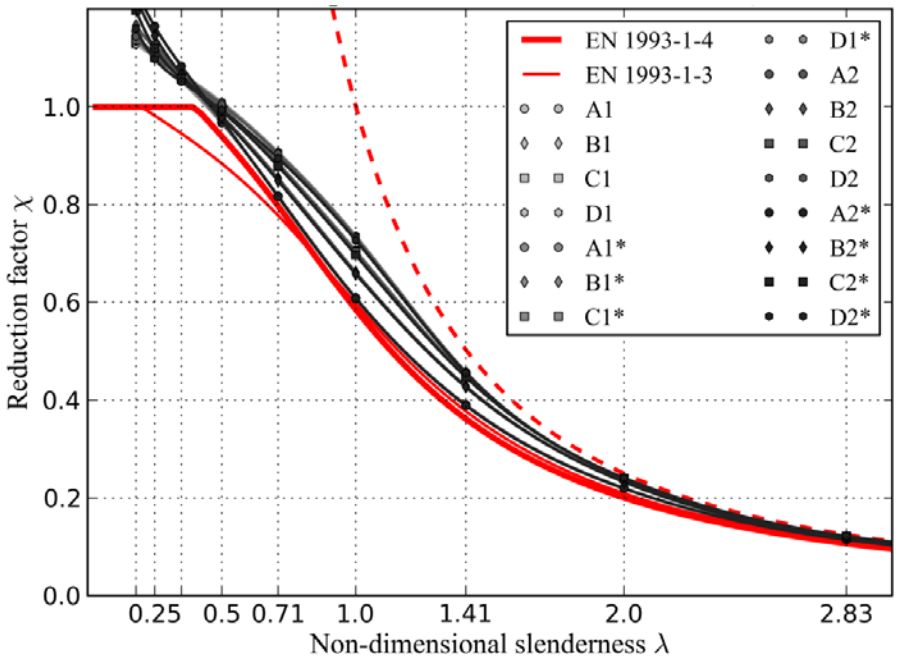

Figure 7 **C 72x34x4 flexural buckling**

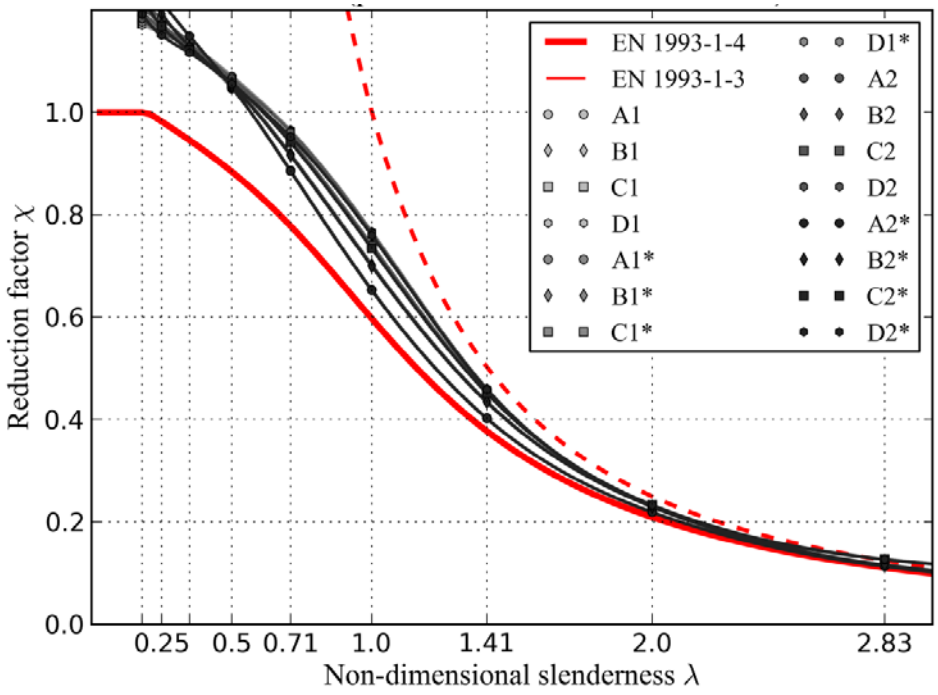

Figure 8 **C 72x34x4 torsional-flexural buckling**

Basic strength can be used together with the EN 1993-1-4 buckling curve in case of flexural and torsional-flexural buckling of the press-braked C-sections (Figures 7 and 8), but the use of average strength provides unsafe results in the case of flexural buckling. For instance, the slenderness 1.0 with the average strength 250 MPa will change to 1.08 for the average strength 294 MPa, but the reduction factor in flexural buckling withl material A1will drop from 0.61 to 0.52, which is lower than the EN 1993-1-4 design curve, where the reduction factor is 0.55. Results are not sensitive to the strain hardening rate, however significant improvement of predicted strength would be possible by increasing the nonlinear factor *n*. The results of the torsional-flexural buckling strength were rather conservative, but this could also be caused by the selection of the cross-sectional shape which was based on compression and bending resistance (particularly the *A*/*W* ratio).

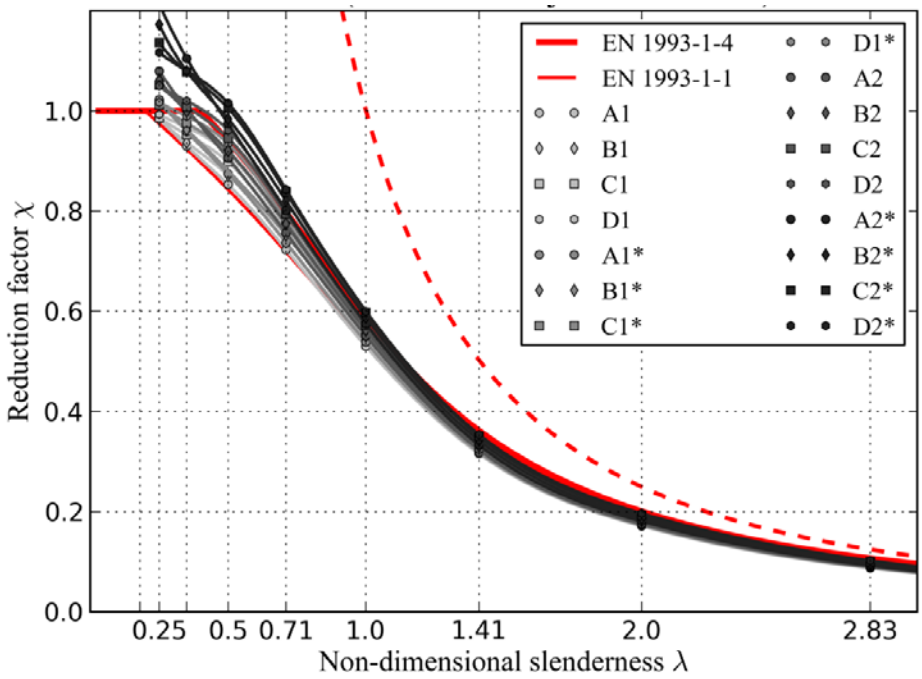

Figure 9 **SHS 48x4 flexural buckling – major axis**

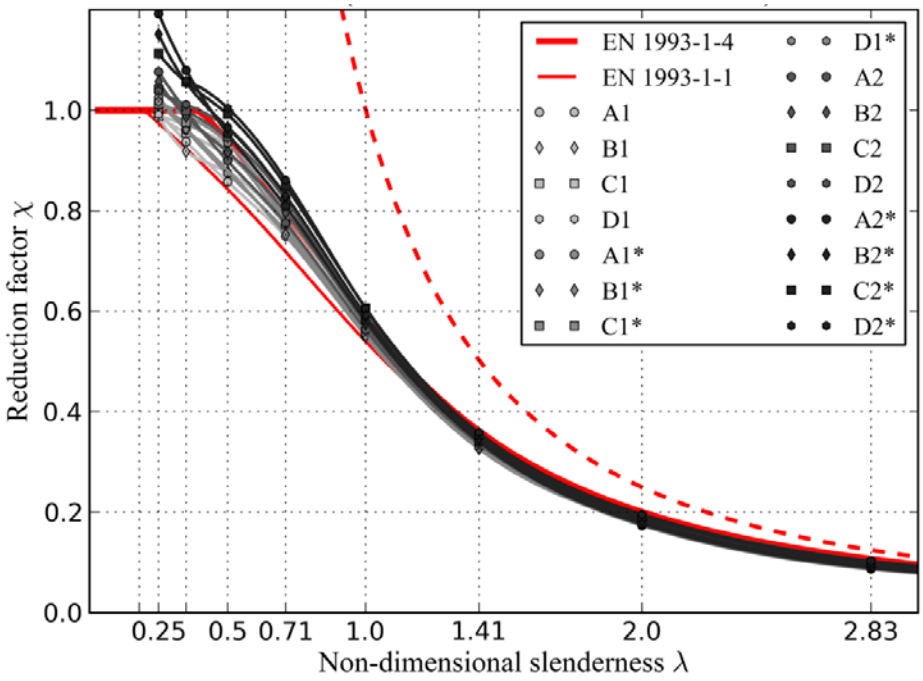

Figure 10 **RHS 72x24x4 flexural buckling – minor axis**

The use of virgin material strength always provides conservative results in cold-rolled hollow sections especially at lower slenderness. A lower buckling strength prediction than the EN 1993-1-4 buckling curve was achieved using material models with a high strain hardening ratio (A1-D1 and A1*-D1*) and the flat parts strength (Figures 9 and 10). However, the results with an average strength are not sensitive to this ratio and they are always unsafe.

6 Conclusions

Welded profiles were tested in major and minor axis flexural buckling and lateral-torsional buckling. The material model was uniform in the whole cross-section with the single material yield strength $f_{y,b}$. The variation of strain hardening ratio f_u/f_y did not significantly affect the results and the effect of the nonlinear parameter n was also relatively small. Calculated results indicate that the current buckling curves for flexural buckling of welded open sections can be used with all materials.

Press-braked channels were tested in minor axis flexural and torsional-flexural buckling. The basic yield strength $f_{y,b}$ and the average strength $f_{y,a}$ were used in evaluation. The use of average strength would require the recalibration of the buckling curve in Eurocode, which is only valid in combination with the basic strength. Designers may also benefit from a higher nonlinear parameter n, which is typical in ferritic stainless steels.

Cold-rolled hollow sections were tested in minor and major axis flexural buckling. Virgin material strength $f_{y,v}$, flat parts strength $f_{y,f}$ and average strength $f_{y,a}$ were used. While the application of virgin strength resulted in conservative results, average strength would require new buckling curves as in the case of press-braked sections. The situation was not so clear with flat parts strength, which is nowadays used in the design code. The calculations were very sensitive to the strain hardening ratio due to the differences in enhanced material yield strength prediction, and models containing materials such as ferritic steels with a lower f_u/f_y ratio produced lower strength than the Eurocode buckling curve, especially in lower slenderness ranges. Using the carbon steel buckling curve with the initial slenderness 0.2 would be more appropriate in such cases.

Acknowledgments

The research leading to these results has received funding from the European Community's Research Fund for Coal and Steel (RFCS) under Grant Agreement No. RFSR-CT-2010-00026, Structural Applications of Ferritic Stainless Steels.

References

[1] Hyttinen V, Design of cold-formed stainless steel SHS beam-columns, University of Oulu Report. University of Oulu Report No. 41; 1994.

[2] Talja A, Salmi P, Design of stainless steel RHS beams, columns and beam-columns, VTT Research Notes. VTT Research Note 1619; 1995.

[3] Gardner L, Nethercot DA. Experiments on stainless steel hollow sections—Part 1: Material and cross-sectional behaviour, Journal of Constructional Steel Research. 2004;60;1291-1318.

[4] Manninen T, SAFSS Work Package 1: Characterization of Stress–Strain Behavior, Outokumpu Research Report; 2012.

[5] Real E, Mirambell E, Estrada I. Shear response of stainless steel plate girders, Engineering Structures 2007;29;1626-1640.

[6] Talja A, Hradil P, SAFSS Work Package 2: Report on model calibration tests, VTT Research Report. VTT-R-06130-12; 2012.

[7] Chauhan M, Solin J, Alhainen J, Manninen T, Lönnqvist C. Cyclic behavior and fatigue of stainless steels, Metallurgia Italiana 2012;9;13-18.

[8] Talja A, Test report on welded I and CHS beams, columns and beam-columns, VTT Research Report. WP31-32-33.3S.05; 1997.

[9] Theofanous M, Gardner L. Testing and numerical modelling of lean duplex stainless steel hollow section columns, Engineering Structures 2009;31;3047-3058.

[10] Hradil P, Talja A, Real E, Mirambell E, SAFSS Work Package 2: Review of available data, VTT Research Report. VTT-R-04651-12; 2012.

[11] Hradil P, Fülöp L, Talja A. Global stability of thin-walled ferritic stainless steel members, Thin-Walled Structures 2012;61;106-114.

[12] Hradil P, Talja A, SAFSS Work package 2: Report on preliminary finite element study, VTT Research Report. VTT-R-04891-12; 2012.

[13] Rasmussen KJR, Rondal J. Strength curves for metal columns, Journal of Structural Engineering 1997;123;721.

[14] Mirambell E, Real E. On the calculation of deflections in structural stainless steel beams: an experimental and numerical investigation, Journal of Constructional Steel Research 2000;54;109-133.

[15] Euro Inox and The Steel Construction Institute, Design Manual For Structural Stainless Steel - Commentary, 3rd ed.; 2007.

[16] Lawson RM, Chung KF, Popo-Ola SO, Structural design to BS 5950-5:1998, Section Properties and Load Tables, SCI-P276; 2002.

[17] Outokumpu Stainless, Austenitic, ferritic and lean duplex metric data sheet, accessed online at < http://www.outokumpu.com/ >; 2012.

[18] Hradil P, Fülöp L, Talja A. Virtual testing of cold-formed structural members, Rakenteiden Mekaniikka /Journal of Structural Mechanics 2011;44;206-217.

[19] Cruise RB, Gardner L. Strength enhancements induced during cold forming of stainless steel sections, Journal of Constructional Steel Research 2008;64;1310-1316.

[20] Rossi B, Degée H, Pascon F. Enhanced mechanical properties after cold process of fabrication of non-linear metallic profiles, Thin-Walled Structures 2009;47;1575-1589.

[21] Gardner L, Cruise RB. Modeling of Residual Stresses in Structural Stainless Steel Sections, Journal of Structural Engineering 2009;135;42-53.

[22] Zhang L, Tong GS. Lateral buckling of web-tapered I-beams: A new theory, Journal of Constructional Steel Research 2008;64;1379-1393.

[23] Becque J, Rasmussen KJR. A numerical investigation of local–overall interaction buckling of stainless steel lipped channel columns, Journal of Constructional Steel Research 2009;65;1685-1693.

[24] Becque J, Rasmussen KJR. Numerical Investigation of the Interaction of Local and Overall Buckling of Stainless Steel I-Columns, Journal of Structural Engineering 2009;135;1349-1356.

[25] Ayrton WE, Perry J. On struts, The Engineer 1886;62;464-465.

[26] Sarawit A, CUTWP Thin-walled section properties, accessed online at
< http://www.ce.jhu.edu/bschafer/cutwp/ > ;2012.

[27] Riks E. An incremental approach to the solution of snapping and buckling problems, International Journal of Solids and Structures 1979;15;529-551.